JOURNAL OF MECHANICAL ENGINEERING AND SCIENCES
ISSN: 2289-4659 e-ISSN: 2231-8380
VOLUME 17, ISSUE 2, 2023, 9474 – 9482
DOI: https://doi.org/10.15282/jmes.17.2.2023.6.0750

اونيۏرسيتي مليسيا ڤهڠ
UNIVERSITI MALAYSIA PAHANG

RESEARCH ARTICLE

Impact of eave and roof pitch on cross ventilation for an isolated building with sawtooth roof

L.K. Moey[1]*, S.K. Cheong[2], A.A. Zobaied[2], V.C. Tai[1], T.F. Go[3] and P.L. Chong[4]

[1] Centre for Modelling and Simulation, Faculty of Engineering, Built Environment & Information Technology, SEGi University, 47810, Selangor, Malaysia
Phone: 03-6145 1777; Fax.: 03-6145 1666
[2] Faculty of Engineering, Built Environment & Information Technology, SEGi University, 47810, Selangor, Malaysia
[3] Centre for Advance Materials and Intelligent Manufacturing, Faculty of Engineering, Built Environment & Information Technology, SEGi University, 47810, Selangor, Malaysia
[4] School of Computing, Engineering & Digital Technologies, Teesside University, Middlesbrough, TS1 3BX, United Kingdom

ABSTRACT - An eave refers to an extension attached to the building roof to protect the interior space from direct solar radiation and improve the performance on cross ventilation. In this study, the impact of eave inclination angle and roof pitch of an isolated sawtooth roof building on cross ventilation were investigated. The eave configurations at either windward or leeward openings were included. 3D steady Reynolds-Averaged Navier-Stokes (RANS) equation in combination with the Shear-Stress Transport model (SST *k-ω* model) was used for the Computational Fluid Dynamics (CFD) simulations. Grid sensitivity study was carried out and the performance of cross ventilation was evaluated based on the non-dimensional velocity magnitude, spatial distribution of pressure coefficient as well as the ventilation rate of the building. For the simulation model with 55° roof pitch, it is observed that a region with high velocity magnitude formed on top of the leeward eave due to the higher roof pitch and presence of the leeward eave. Results also indicated that the building model with 90° leeward eave and 55° roof pitch has the highest increment in ventilation rate which is 7.16%. On the other hand, the building model with 90° windward eave has the highest pressure coefficient because more blockage of airflow is caused by a steeper roof as the roof pitch of the building increases. Furthermore, the building model with 90° leeward eave shows a larger region with negative pressure at the leeward façade indicating higher airflow leaving the leeward opening. Therefore, the airflow behavior and characteristic are both dependent on the roof pitch and eave inclination angle for a naturally ventilated building.

ARTICLE HISTORY
Received : 23rd Dec. 2022
Revised : 17th May 2023
Accepted : 04th June 2023
Published : 28th June 2023

KEYWORDS
CFD
Cross ventilation
Eave inclination
Roof pitch
Ventilation rate

1.0 INTRODUCTION

Natural ventilation is a passive way of cooling which is environmental-friendly in supplying fresh air and creating a preferred environment within a building [1]. Natural ventilation is usually recommended for buildings as it requires relatively low operating and maintenance expenses as compared to the mechanical ventilation. The growth for the usage of mechanical ventilation has impacted the Earth in terms of the quantum leap of the world energy consumption. In Malaysia, there is a drastic increment in the energy consumption among the residential sector which mainly contributed by the high usage of HVAC equipment such as the air-conditioner. This is due to the operation of HVAC equipment which requires high consumption of electricity. The total electricity consumption in residential and commercial sector of Malaysia increased by 100% from 2000 to 2018 [2]. Thus, natural ventilation is crucial to act as an alternative method in residential sector to reduce the electricity demand in the community. Cross ventilation is proven to improve the air quality of the indoor environment and also the indoor thermal comfort [3].

In CFD simulations, the RANS method is commonly employed to predict the airflow field. Ntinas et al. [4] validated various 3D turbulence models for predicting airflow patterns around arched-type, pitched-type, and flat-type roof agricultural buildings using wind tunnel experiments. The study found that the Standard *k-ε*, RNG *k-ε*, and Realizable *k-ε* models showed good agreement in predicting velocity contours. Nimarshana et al. [5] highlighted the importance of strategically selecting wind tunnel data for CFD model validation to accurately predict airflow and thermal comfort. Nasrollahi et al. [6] examined how the height of openings impacts natural airflow in high-rise buildings for thermal comfort and energy efficiency. The field studies and numerical modeling suggest that the appropriate location of openings is crucial to improve thermal comfort in hot climates.

Perén et al. [7] investigated an isolated building characterized with symmetric and asymmetric opening. The results demonstrated that the roof tilt angles of a sawtooth roof can affect the airflow characteristics such as the velocity, airflow pattern and pressure coefficient around the building. Moreover, it was also indicated that obstacle and blockage near the

***CORRESPONDING AUTHOR | L. K. Moey** | ✉ moeylipkean@segi.edu.my

window opening should be avoided for higher volume flow rate. Chu and Chiang found that the ventilation rate of the low rise building with internal obstacle reduces when an obstacle is placed adjacent to either inlet or outlet opening [8]. Furthermore, a numerical study conducted by Moey et al. [9] found out that the ventilation rate in the building increases as the roof pitch increases via the analysis of the airflow characteristic around and inside a building with various gable roof angles of 15°, 25° and 35°.

Eave can be described as part of the roof which is commonly seen for building, and it acts as a protection against the radiation from solar. Thus, eave can be adopted for building because it provides solar shading which is able to minimize the air- conditioner usage and subsequently lower the building electricity consumption. A study by Perén et al. [10] found out that the inclination angle of windward eave lower than 0° can improve the volume flow rate within the building. Additionally, it was discovered that eave can be deployed to increase the flow inside the building. However, Perén et al. [10] only focused on the impact of eave inclination without considering the effect of roof angle on building cross ventilation. Furthermore, sawtooth roof is characterized by the windward opening with a lower position and the leeward opening with a higher position [11]. Cui [12] performed a wind tunnel test to evaluate the wind pressure coefficient on the sawtooth roof buildings. The experimental results demonstrated that increasing the distance between sawtooth roofs lead to higher peak negative wind pressure on the sawtooth roof. Similar testing has been conducted by Li et al. [13], it was discovered that sawtooth roof experienced higher peak design pressure coefficient with increasing roof slope. Furthermore, the findings suggested that the current provisions for wind pressure design of sawtooth roof may underestimate the critical wind suction. These findings support the notion that sawtooth roof are a promising research avenue, as further demonstrated by a recent CFD study examining the impact of sawtooth roof inclination angles and asymmetrical opening positions for an isolated building in cross ventilation [14]. Accordingly, this paper aims to continue this CFD research direction by examining the effects of roof pitches and eaves inclination on cross ventilation. As such, the main contribution of this paper is to provide more comprehensive insights into the ventilation effect of sawtooth roof.

This paper consists of the 4 sections. Section 2 describes the methodology such as model setup, numerical setting, and grid sensitivity study. Section 3 discusses the results for the sawtooth roof building with different roof pitches and eaves inclination. Lastly, the conclusion of this study will be presented in section 4.

2.0 METHODOLOGY

2.1 Building Model, Simulation Cases, Computational Domain and Grids

The basic building model from Karava et al. [15] with the 0.1 m × 0.1 m × 0.08 m [length (L) × width (W) × height (H)] dimensions was referred in this study. This basic building model was used for the purpose of grid sensitivity study. Furthermore, the reference model with sawtooth roof from Perén et al. [10] which has a 1:60 reduced scale dimensions of 0.1 m × 0.05 m × 0.095 m ($L \times W \times H$) was selected for this study. The reference model has a pair of window (h = 0.01 m) at windward and leeward walls, with the bottom of the windward opening at y = 0.024 m and the bottom of leeward opening at y = 0.077 m. The thickness of the wall and the ground for the model was 0.004 m and 0.006 m, respectively. A sawtooth roof with various roof pitches and different eaves inclination with a fixed length L = 0.025 m were added to the simulation model. The simulation model was investigated with five various roof pitches of 15°, 25.5°, 35°, 45° and 55° with inclination of windward eaves (WE) namely 90°, -27° and -45° as well as inclination of leeward eaves (LE) at 90°. The dimensions of the sawtooth roof model with 25.5° roof pitch is shown in Figure 1 while the simulation cases with various roof pitches and eaves inclination angle that were conducted in this study is shown in Table 1.

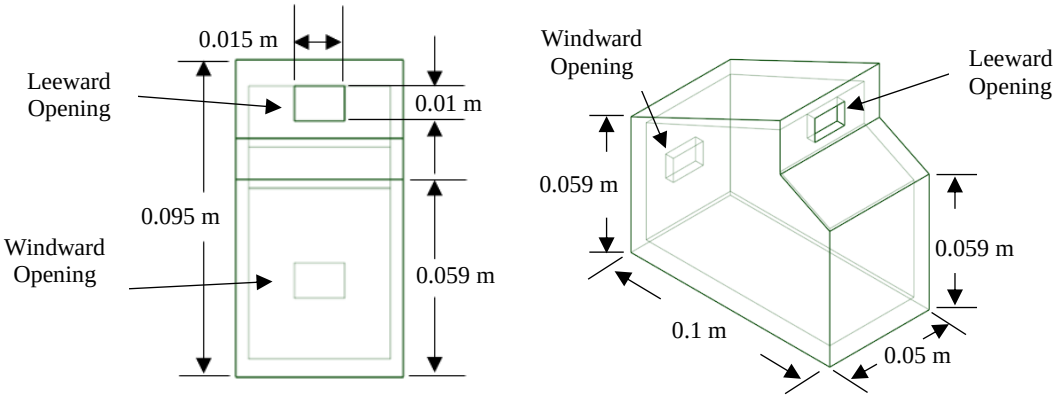

Figure 1. Sawtooth roof model with 25.5° roof pitch: (a) Side view and (b) Isometric view with dimensions

Table 1. Simulation cases of sawtooth roof model

Cases	Roof Pitches (°)	Eaves Inclination Angle (°)
Case 1	15.0	90 (WE)
Case 2	25.5	90 (WE)
Case 3	35.0	90 (WE)
Case 4	45.0	90 (WE)
Case 5	55.0	90 (WE)
Case 6	15.0	-27 (WE)
Case 7	25.5	-27 (WE)
Case 8	35.0	-27 (WE)
Case 9	45.0	-27 (WE)
Case 10	55.0	-27 (WE)
Case 11	15.0	-45 (WE)
Case 12	25.5	-45 (WE)
Case 13	35.0	-45 (WE)
Case 14	45.0	-45 (WE)
Case 15	55.0	-45 (WE)
Case 16	15.0	90 (LE)
Case 17	25.5	90 (LE)
Case 18	35.0	90 (LE)
Case 19	45.0	90 (LE)
Case 20	55.0	90 (LE)

WE = windward eaves, LE = leeward eaves

The top and side walls of the computational domain were 5H from the building model, as shown in Figure 2. The distance from the leeward side of the building model to the outlet was 15H, of which H is the height of the building. The computational domain was created with reference to Franke et al. [16] and Tominaga et al. [17] with the exception that the distance from the inlet to the windward side of the building model has been decreased from 5H to 3H to restrict the amount of unintentional streamwise gradient [18].

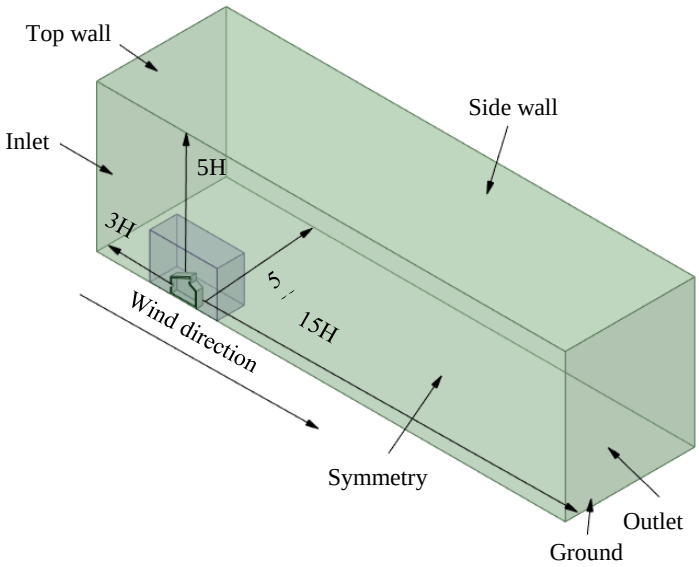

Figure 2. Dimensions of the computational domain used in this study

Mosaic™ meshing technology was used to generate the computational grids. It can produce the good quality octree hexahedron in the bulk region and allows automatic connection of elements [19]. Based on the curvature, proximity, and soft size requirements, the model geometry and computational domain were both remeshed with tetrahedral elements using the local scope sizing function. The mesh type was then converted into Poly-hexcore type by preserving its average edge length consistency with triangular surface mesh as shown in Figure 3 [19].

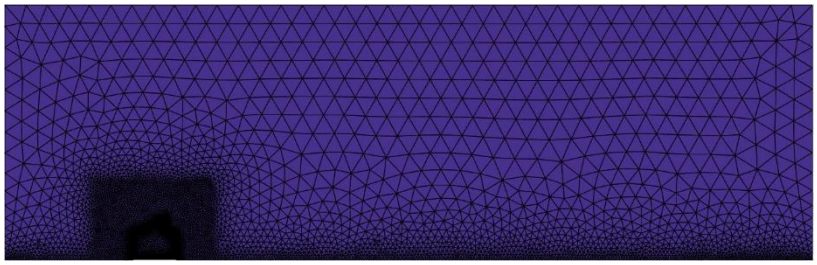

(a)

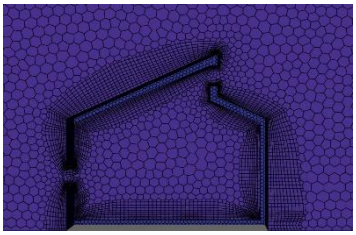

(b) (c)

Figure 3. (a) Triangular surface mesh, (b) Poly-hexcore mesh with a close-up view and (c) inflation layers generated for the reference model

2.2 Boundary Conditions

At the inlet plane, the boundary condition of measured mean wind speed and turbulent intensity from the wind tunnel experiment were used. The Eq. (1) was used to determine the wind velocity profile at the inlet.

$$U(z) = \frac{u^*_{ABL}}{K} ln(\frac{z + z_0}{z}) \quad (1)$$

where, z_0 = 0.1 m, and u^*_{ABL} was computed using the reference wind speed, U_{Ref} of 6.97 m/s, reference height, Z_{Ref} of 0.08 m, Von Karman constant, κ of 0.42, and the aerodynamic roughness height Z_0 of 0.00003 m [20].

The Eq. (2) was used to to calculate the turbulent kinetic energy *k(z)* at reference height.

$$k(z) = \alpha \, (I_u \, (z) U(z))^2 \quad (2)$$

where, U(z) is the mean wind speed, I_u(z) is the turbulent intensity and α = 0.5 [21,22]

The Eq. (3) was used to determine the rate of turbulence dissipation ε.

$$\mathcal{E}(z) = \frac{u^{*3}_{ABL}}{\kappa(z + z_0)} \quad (3)$$

The Eq. (4) was used to determine the specific dissipation rate.

$$\omega(z) = \frac{\varepsilon(z)}{C_\mu k(z)} \quad (4)$$

where, C_μ is the empirical constant equivalent to 0.09 [18].

For ground and building surfaces, standard wall functions developed by Launder & Spalding and sand-grain based roughness modification from Cebeci & Bradshaw's were utilized [23,24]. The values of roughness parameters such as sand-grain roughness height, k_s and roughness constant, C_s were computed in accordance to their relation to z_0 which has been obtained through the study of Ramponi and Blocken [18]. The ground sand-grain roughness height, k_s = 0.00028 m was atttained through Eq. (5). The standard wall functions were also applied for building surface with k_s = 0.

$$k_s = \frac{9.793 z_0}{C_s} \quad (5)$$

where, the roughness constant, C_s was set at 0.874.

At the symmetry and the outlet plane, zero static pressure was applied. At the top and side planes, zero normal gradients and velocity corresponding to zero shear condition were also imposed.

2.3 Solver Settings

ANSYS 2021 R2 was utilized for the numerical simulations in this study. The 3D steady RANS equation was solved using the SST *k-ω* turbulence model. The SIMPLE algorithm based on Green Gauss node spatial discretization was used. Both convection and viscous terms of the governing equation were also utilized for the second order upwind discretization

and pressure interpolation. Convergence was achieved as the scaled residuals recede downward towards 10^{-6} for x, y momentum, 10^{-5} for z momentum and 10^{-4} for continuity, k and ω.

2.4 Grid Sensitivity Study

Grid sensitivity study was carried out for the basic building model. Three different cell counts were used which include 507,859 cells (grid A), 935,682 cells (grid B), and 1,125,393 cells (grid C) in order to make sure that the result is grid independent. The simulations were performed to generate a graph of mean streamline velocity ratio (U/U_{Ref}) of which U refers to 3D streamwise velocity vector, while U_{ref} = 6.97 m/s represents the reference wind speed measured at the height of the building (H = 0.08 m). Results of these three grids were compared with the PIV experiment results from [15] as shown in Figure 4. Grid sensitivity study indicates that data generated from the medium grid (grid B) simulation best replicates results obtained by Karava et al. [15]. Therefore, the grid B was selected for all successive simulations for this study.

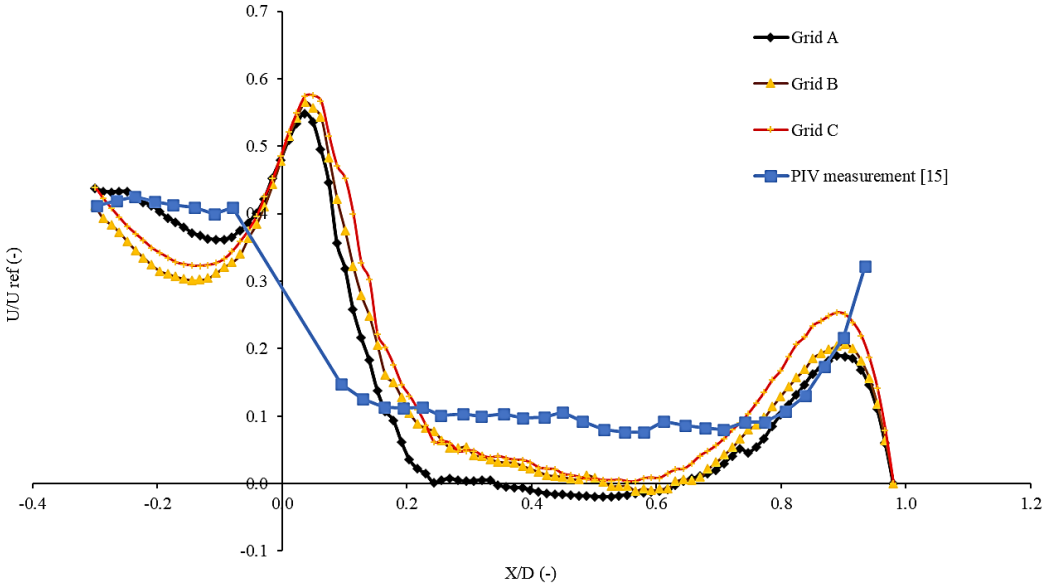

Figure 4. Comparison of the three different cell counts for grid A (coarse), grid B (medium) & grid C (fine) with result of PIV measurement by Karava et al. [15]

3.0 RESULTS AND DISCUSSION

3.1 Non-Dimensional Velocity Magnitude

Table 2 illustrates the contour plots of non-dimensional velocity magnitude for different roof pitches and eaves inclination. The contours for the 90° windward and leeward eaves indicate that there is a change in direction for the inlet airflow which deflected to slightly downward direction and the recirculation of the airflow occurs and is getting larger within the simulation model as the roof pitch increases. On the contrary, for the -45° windward eave, the incoming airflow has a slightly upward direction and the recirculation of airflow is observed and becomes larger before leaving the simulation model as the roof pitch increases. Thus, the changes in the inlet air flow direction corresponds to the distribution of static pressure that has been adjusted in the area of the windward façade. This observation is consistent with the findings from the literature [10]. Furthermore, recirculation zone formed under the windward eaves of -27° and -45° were observed to be obstructed to the airflow for reaching up to the leeward opening. Additionally, the presence of the eave with 55° roof pitch results in a region with high-velocity magnitude forming on top of the leeward eave.

Table 2. Non-dimensional velocity magnitude of various roof pitches and eaves inclination

Cases	Legend	15°	25.5°	35°	45°	55°
90º Windward Eave	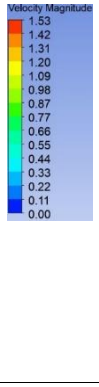	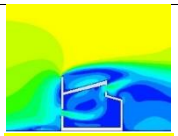	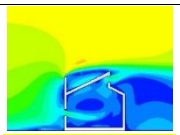	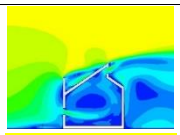	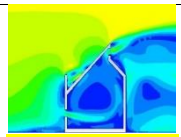	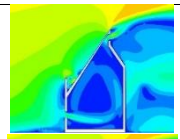
-27º Windward Eave		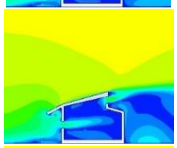	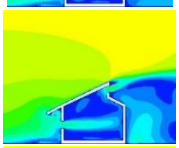	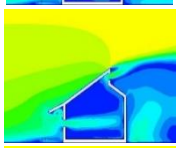	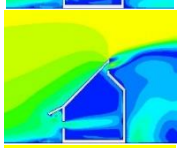	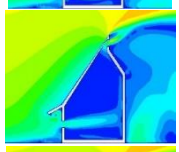
-45º Windward Eave		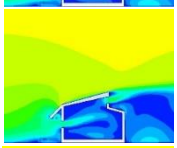	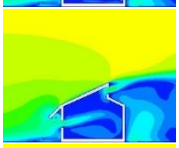	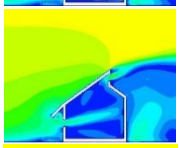	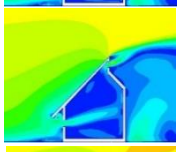	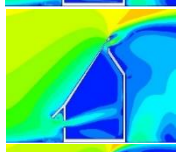
90º Leeward Eave		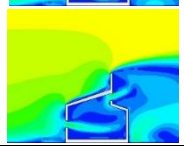	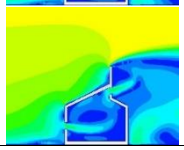	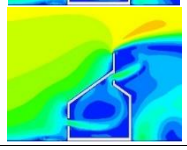	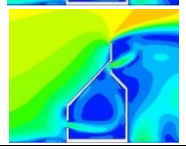	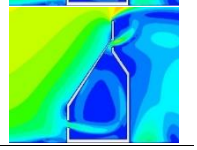

3.2 Spatial Distribution of Pressure Coefficient

Table 3 shows the spatial distribution of pressure coefficient around the simulation model having various roof pitches as well as different windward (WE) and leeward (LE) eaves inclination namely 90º WE, -27º WE, -45º WE and 90º LE. Observation shows that the simulation model with 90° WE produces the highest positive peak value of pressure coefficient among all the simulation cases. Furthermore, positive pressure coefficient also occurs around the smilation model attached with 90° LE because of the flow separation at the top region of the eaves. Spatial distribution of the pressure coefficient for -27° and -45° WE increases as the roof pitch increases. However, it is observed for all simulation cases, the negative value of pressure coefficient at the leeward façade of the roof increases significantly as the roof pitch increases, causing a greater region of wake formation to form.

Table 3. Spatial distribution of pressure coefficient for various roof pitches and eaves inclination

Cases	Legend	15°	25.5°	35°	45°	55°
90º Windward Eave	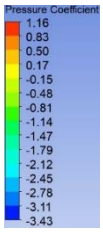	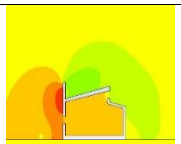				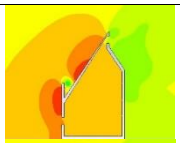
-27º Windward Eave						
-45º Windward Eave			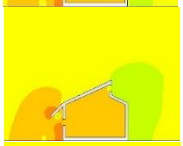			
90º Leeward Eave		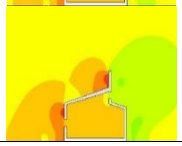				

3.3 Ventilation Rate

A simple relationship can be deployed to calculate the building ventilation rate. The ventilation rate of an isolated cross-ventilated roof building can be calculated from the following Eqs. [25]:

$$C_p = \frac{p - p_r}{\frac{1}{2}\rho V_{ref}^2} \tag{6}$$

$$CQ = C_d V_{ref} \sqrt{\Delta C_p} \tag{7}$$

$$C_a = \frac{CQ}{(1+CQ)} \tag{8}$$

$$Q = C_a V_{ref} A_e \tag{9}$$

Eq. (6) can be applied to calculate the pressure coefficient, C_P, in which P refers to the pressure exists at designated opening, P_r represents the reference free stream static pressure, $\rho = 1.225$ kg/m^3 represents the air density, and $V_{ref} = 6.97$ m/s. This pressure coefficient calculated at both windward and leeward openings were then used in Eq. (7) to determine the estimated flow coefficient CQ, in which $C_d = 0.62$ represents the discharge coefficient of a sharp opening while Δ_{CP} represents the change of pressure coefficient between the windward and leedward openings. The actual flow coefficient, C_a was calculated by using Eq. (8). Subsequently, Eq. (9) can be used to compute the ventilation rate by multiplying the actual flow coefficient C_a, with V_{ref}, and effective area of opening A_e. The effective area A_e was calculated to be 1.575×10^{-4} m^2 in this study.

Figure 5 shows the percentage difference for the ventilation rate between each simulation case and the reference model. Result demonstrates that ventilation rate increases as the roof pitch increases. For the simulation models attached with -27° and -45° WE, the ventilation rate reduces as the roof pitch is in the range of 15° and 35°. However, the ventilation rate increases as the roof pitch increases to the range of 45° and 55°. For -27° WE, the ventilation rate increases by 1.05% and 5.12% for the roof pitch of 45° and 55°, respectively. Similarly, with the roof pitch of 45° and 55°, the ventilation rate for -45° WE improve by 0.52% and 3.66%, respectively. Additionally, the ventilation rate increses as compared to the reference model for all the simulation cases with 90° LE regardless of the roof pitch. On the other hand, roof pitch of 55° has the greatest improvement of ventilation rate regardlesss of the eave orientation. Also, except for the 90° LE, the ventilation rate reduces for the roof pitch of 15° and 25.5°. Moreover, 90° LE with 55° roof pitch has the greatest improvement of ventilation rate up to 7.16%. This is consistent with the non-dimensional velocity magnitude contours shown in Table 2 earlier. This is due to the fact that as the airflow velocity in the simulation model increases, the ventilation rate increases along with the increment in roof pitch.

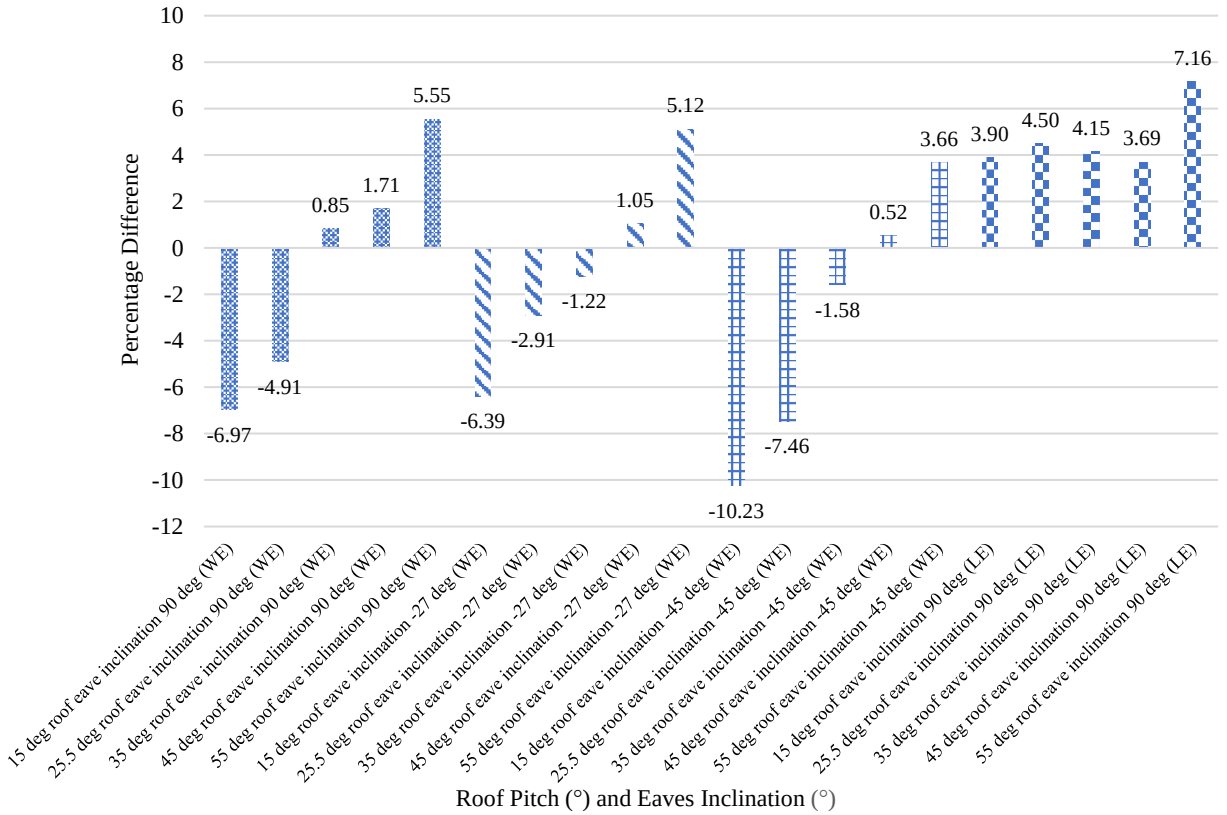

Figure 5. Percentage difference for the ventilation rate between each simulation case and the reference model

4.0 CONCLUSION

This paper investigated and analyzed the airflow characteristics around and within an isolated building with sawtooth roof of different roof pitch (15º, 25.5º, 35º, 45 º & 55°) and various eaves inclination (90º WE, -27º WE, -45º WE and 90º LE) using 3D steady-state RANS equation with SST $k-\omega$ turbulence model. Numerical result shows that the non-dimensional velocity magnitude, pressure coefficient, and ventilation rate are significantly dependent on both roof pitches and eave inclination angles. It is observed that the incoming airflow for the 90º windward and leeward eaves deflected slightly downward. In contrast, for the -45º windward eave, the airflow deflected slightly upward. Furthermore, the

ventilation rate increses as compared to the reference model for all the simulation cases with 90° LE regardless of the roof pitch. Ventilation rate is an important indicator when it comes to assess the performance on building ventilation. As the conclusion, the sawtooth roof with steeper roof pitch and attached with 90° leeward eave has the highest ventilation rate among all simulation cases. Because different wind speed values, opening positions, and additional obstacles within the building can influence the ventilation rate, such factors can beinvestigated further in future study.

5.0 REFERENCES

[1] C. H. Lim, S. Omidreza, S. Kamaruzzaman, M. Y. Sulaiman, M. Sohif, S. Elias, and K.C. Ng, "Design configurations analysis of wind-induced natural ventilation tower in hot humid climate using computational fluid dynamics," *International Journal of Low-Carbon Technologies*, vol. 10, no. 4, pp. 332–346, 2015.

[2] Energy Data and Research Unit, *Malaysia Energy Statistics Handbook*, Putrajaya, Malaysia: Suruhanjaya Tenaga (Energy Commission), pp. 86, 2020, [Online]. Available: www.st.gov.my

[3] L. K. Moey, N. M. Adam, K. A. Ahmad, and L. C. Abdullah, "Wind tunnel study of different roof geometry configurations for wind induced natural ventilation into stairwell in tropical climate," *International Journal of Applied Engineering Research*, vol. 13, no. 5, pp. 2635–2647, 2018.

[4] G. K. Ntinas, X. Shen, Y. Wang, and G. Zhang, "Evaluation of CFD turbulence models for simulating external airflow around varied building roof with wind tunnel experiment," *Building Simulation*, vol. 11, pp. 115-123, 2018.

[5] P. H. V. Nimarshana , R. A. Attalage, and K. K. C. Perera, "Quantification of the impact of RANS turbulence models on airflow distribution in horizontal planes of a generic building under cross-ventilation for prediction of indoor thermal comfort," *Journal of Building Engineering*, vol. 52, pp. 104409, 2022.

[6] N. Nasrollahi and P. Ghobadi, "Field measurement and numerical investigation of natural cross-ventilation in high-rise buildings; Thermal comfort analysis, " *Applied Thermal Engineering*, vol. 211, pp. 118500, 2022.

[7] J. I. Perén , T. van Hooff, R. Ramponi, B. Blocken, and B. C. C. Leite, "Impact of roof geometry of an isolated leeward sawtooth roof building on cross-ventilation: Straight, concave, hybrid or convex?," *Journal of Wind Engineering and Industrial Aerodynamics*, vol. 145, pp. 102–114, 2015.

[8] C. R. Chu and B. F. Chiang, "Wind-driven cross ventilation with internal obstacles," *Energy and Buildings*, vol. 67, pp. 201–209, 2013.

[9] L. K. Moey, M. F. Kong, V. C. Tai, T. F. Go, and N. M. Adam, "Effect of Gable roof angle on natural ventilation for an isolated building," *Jordan Journal of Mechanical & Industrial Engineering*, vol. 15, no. 3, pp. 291–300, 2021.

[10] J. I. Perén, T. van Hooff, B. C. C. Leite, and B. Blocken, "Impact of eaves on cross-ventilation of a generic isolated leeward sawtooth roof building: Windward eaves, leeward eaves and eaves inclination," *Building and Environment*, vol. 92, pp. 578–590, 2015.

[11] J. I. Perén, T. Van Hooff, B. C. C. Leite, and B. Blocken, "CFD simulation of wind-driven upward cross ventilation and its enhancement in long buildings: Impact of single-span versus double-span leeward sawtooth roof and opening ratio," *Building and Environment*, vol. 96, pp. 142-156, 2015.

[12] B. Cui, "Wind effects on monosloped and sawtooth roofs," *Ph.D Thesis*, Clemson University, 2007.

[13] C. Li, Y. Han, J. Zhang, S. Liu, and C. S. Cai, "Wind tunnel tests on wind pressure characteristics of sawtooth roofs, " *Journal of Aerospace Engineering*, vol. 31, no. 6, pp. 04018107, 2018.

[14] O. H. Al-Aghbari, L. K. Moey, V. C. Tai, T. F. Go, and M. H. Yazdi, "Study on the impact of sawtooth roof inclination angles and asymmetrical opening positions for an isolated building in cross ventilation, " *Jordan Journal of Mechanical & Industrial Engineering*, vol.16, no. 5, pp. 865-878, 2022.

[15] P. Karava, T. Stathopoulos, and A. K. Athienitis, "Airflow assessment in cross-ventilated buildings with operable façade elements," *Building and environment*, vol. 46, no. 1, pp. 266–279, 2011.

[16] J. Franke, A. Hellsten, H. Schlünzen, and B. Carissimo, "Best practice guideline for the CFD simulation of flows in the urban environment," *COST Action*, vol. 44, pp. 1–52, 2007.

[17] Y. Tominaga, A. Mochida, R. Yoshie, H. Kataoka, T. Nozu, M. Yoshikawa, and T. Shirasawa, "AIJ guidelines for practical applications of CFD to pedestrian wind environment around buildings," *Journal of Wind Engineering and Industrial Aerodynamics*, vol. 96, no. 10–11, pp. 1749–1761, 2008.

[18] R. Ramponi and B. Blocken, "CFD simulation of cross-ventilation for a generic isolated building: Impact of computational parameters," *Building and Environment*, vol. 53, pp. 34–48, 2012.

[19] K. Zore, B. Sasanapuri, G. Parkhi, and A. Varghese, "Ansys mosaic poly-hexcore mesh for high-lift aircraft configuration," *21st Annual CFD Symposium*, Bangalore, August 2019.

[20] P. Karava, "Airflow prediction in buildings for natural ventilation design: Wind tunnel measurements and simulation," *Ph.D Thesis*, Concordia University, 2008.

[21] R. Ramponi and B. Blocken, "CFD simulation of cross-ventilation flow for different isolated building configurations: Validation with wind tunnel measurements and analysis of physical and numerical diffusion effects," *Journal of Wind Engineering and Industrial Aerodynamics*, vol. 104–106, pp. 408–418, 2012.

[22] Y. Tominaga, S. ichi Akabayashi, T. Kitahara, and Y. Arinami, "Air flow around isolated gable-roof buildings with different roof pitches: Wind tunnel experiments and CFD simulations," *Building and Environment*, vol. 84, pp. 204–213, 2015.

[23] B. E. Launder and D. B. Spalding, "The numerical computation of turbulent flows," *Computer Methods in Applied Mechanics and Engineering*, vol. 3, no. 2, pp. 269–289, 1974.

[24] T. Cebeci and P. Bradshaw, "Momentum transfer in boundary layers," *New York: Hemisphere Publishing Corporation*, 1977.

[25] M. Swami and S. Chandra, "Procedures for calculating natural ventilation airflow rates in buildings," *ASHRAE Final Report FSEC-CR-163-86*, 1987.